Journal of Ceramic Processing Research. Vol. 4, No. 4, pp. 197~201 (2003)

J O U R N A L O F
Ceramic Processing Research

Synthesis and characteristics of ultrafine hydroxyapatite particles

Yosuke Tanaka, Yoshihiro Hirata* and Ryuichi Yoshinaka

Department of Advanced Nanostructured Materials Science and Technology, Graduate School of Science and Engineering, Kagoshima University, 1-21-40 Korimoto, Kagoshima 890-0065, Japan

Ultrafine hydroxyapatite powders ($Ca_{10}(PO_4)_6(OH)_2$) with 40-90 m^2/g specific surface area were synthesized by the reaction between $Ca(OH)_2$ suspensions and H_3PO_4 solutions at room temperature. The influence of the size of the starting $Ca(OH)_2$ powder, mixing rate and concentration of starting raw materials on the characteristics of the hydroxyapatite powder produced were studied by X-ray powder diffraction, infrared spectroscopy, specific surface area measurements and transmission electron microscopy. The reproducibility of experimental results was also investigated. When a H_3PO_4 solution was added once to a $Ca(OH)_2$ suspension, the reproducibility of the result became lower. An increase in the concentrations of the starting raw materials promoted the formation of ultrafine needle-shape hydroxyapatite particles with smaller crystallite size and higher specific surface area. The characteristics of the hydroxyapatite produced did not depend on the size of starting $Ca(OH)_2$ powder.

Key words: Hydroxyapatite, Specific surface area, Nanometer-sized particles, Crystallite.

Introduction

Hydroxyapatite (HAp, $Ca_{10}(PO_4)_6(OH)_2$) ceramics have been used as a prosthesis of human bone or teeth because HAp is an inorganic component of the human bone and has a high bioactivity and biocompatibility [1]. A comparison of mechanical properties between human bone and typical bioceramics is shown in Table 1 [2-4]. HAp ceramics have a comparable flexural strength to human bone. However, the elastic modulus and compressive strength of HAp ceramics are higher than those of human bone, while the fracture toughness is significantly higher for human bone than for HAp ceramics. A similar tendency is observed for tri-calcium phosphate (TCP, $Ca_3(PO_4)_2$) ceramics. Compared with human bone, the alumina ceramics developed have a higher elastic modulus and strength. The mechanical properties of HAp ceramics can approach those of human bone by decreasing the elastic modulus and by increasing the fracture toughness. This improvement may be achieved by making a fibrous collagen-reinforced HAp matrix composite whose structure is very similar to that of human bone. The HAp matrix should contain micropores to run small blood vessels after the implant in human body. To maintain the mechanical strength of the HAp matrix with micropores, the shape and size of the pores need to be strictly controlled. On the other hand, it is well known that the strength of dense ceramics increases when the grain size becomes smaller. That is, a 1st step to develop an improved bioceramics is to make a fine-grained strong apatite ceramics with controlled micropores. In this paper, the preparation of ultrafine hydroxyapatite particles was studied to produce improved bioceramics with the microstructure described. The driving force for sintering of ceramics is the surface energy of raw powder. The distance of material transport during the sintering becomes shorter for an ultrafine powder with a high specific surface area, resulting in a densification at a low temperature. Therefore, a low temperature sintering is effective to produce fine-grained apatite ceramics because of a low grain growth rate. Table 2 summarizes the reported synthesis methods of hydroxyapatite powder. In No.1 [5] and No.2 [6], $Ca(OH)_2$ and $H_3(PO)_4$ were used as raw materials to produce spherical-shape particles (No.1) and needle-shape particles (No.2). The synthesis temperature affects the shape of the particles produced. In the methods of No.3 [7] and No.4 [8] with $Ca(NO_3)_2$ and $NH_4H_2PO_4$, needle-shape particles were produced. The methods No.5 [9] and No.6 [10] gave spherical-shape particles and needle-shape particles, respectively. For the low temperature sintering, a small particle size, a narrow particle size

Table 1. Comparison of mechanical between human bone and bioceramics

Materials	Elastic modulus (GPa)	Compressive strength (MPa)	Flexural strength (MPa)	Fracture toughness ($MPa \cdot m^{1/2}$)
Human bone	7-30	100-300	50-150	2-6
HAp* ceramics	86-110	500-1000	115-200	1
TCP** ceramics	30-90	400-700	130-160	1
Al_2O_3 ceramics	300-400	4500	550	3-5

*Corresponding author:
Tel : (+81) 99-285-8325
Fax: (+81) 99-257-4742
E-mail: hirata@apc.kagoshima-u.ac.jp

Table 2. Synthesis methods of hydroxyapatite

Synthesis method	Ca source	P source	Chemical reaction	Specific surface area (m^2/g)	Particle size (nm)	Reference
No.1	0.5M-$Ca(OH)_2$	0.3-M H_3PO_4	$10Ca(OH)_2+6H_3PO_4\rightarrow Ca_{10}(PO_4)_6(OH)_2+18H_2O$	50	60	5
No.2	1.67M-$Ca(OH)_2$	1.0-M H_3PO_4	$10Ca(OH)_2+6H_3PO_4\rightarrow Ca_{10}(PO_4)_6(OH)_2+18H_2O$	57.5	width 15-25 length 100-200	6
No.3	0.5M-$Ca(NO_3)_2$	0.6-M $NH_4H_2PO_4$	$10Ca(NO_3)_2+6NH_4H_2PO_4+8NH_4OH\rightarrow Ca_{10}(PO_4)_6(OH)_2+20NH_4NO_3+6H_2O$	–	50	7
No.4	0.5M-$Ca(NO_3)_2$	0.6-M $NH_4H_2PO_4$	$10Ca(NO_3)_2+6NH_4H_2PO_4+8NH_4OH\rightarrow Ca_{10}(PO_4)_6(OH)_2+20NH_4NO_3+6H_2O$	40	25	8
No.5	0.05M-$Ca(NO_3)_2$	$P(OC_2H_5)_3$	–	–	10	9
No.6	β-tricalcium phosphote & citric acid		–	–	width 0.1-1 μm length 20-30 μm	10

distribution, a high dispersibility of primary particles and a round shape of particles are desired. The purpose of this research is to synthesize a nanometer-sized HAp powder with the desired properties.

Experimental Procedure

In this experiment, $Ca(OH)_2$ and $H_3(PO)_4$ were used as raw materials to produce apatite particles according to the reaction of No. 1 in Table 2. Calcium hydroxide with specific surface areas of 69.4 $m^2 \cdot g^{-1}$ (sample A, Wako Pure Chemical Industries, Ltd. Tokyo, Japan) and 14.3 $m^2 \cdot g^{-1}$ (sample B, Shiraishi Kogyo Kaisha, Ltd. Hyogo, Japan) was dispersed to make the suspensions of 0.5-3.0 M $Ca(OH)_2$. The 100 ml of 0.3-1.8 M orthophosphoric acid solution was added to a 100 ml of calcium hydroxide suspension at a rate of 1 ml/minute or at one time. The pH value of the mixed suspension was monitored by a pH meter (M-11, Horiba Co. Tokyo, Japan) during the addition of the orthophosphoric acid solution. The apatite powder produced was aged for 24 h. Then, the apatite particles in the suspension were filtrated, washed with ethanol three times, and dried at 100°C for 24 h in air. Some of the aqueous suspensions produced were freeze-dried to make a dispersible apatite powder (FRD-50M, Iwaki Glass Co. Ltd. Tokyo, Japan). The phases produced in the synthesized powder were identified by X-ray powder diffraction (No. 2013, Rigaku Co. Tokyo, Japan) under the following measurement conditions: tube target: Cu, filter: Ni, power voltage: 40 kV, current: 30 mA, scan speed: 2°/minute, chart speed: 2 cm/minute. The size (D) of apatite crystallite was determined from the Scherrer equation, $D(h\ k\ l)=K\lambda/B\cos\theta$, where (h k l) is the Miller indices, K the constant (~0.9), λ the X-ray wavelength (0.154178 nm) and θ the Bragg angle. The line broadening, B, is given at half the peak height. In this experiment, the diffraction line from (002) was used to determine the crystallite size. Infrared spectra were measured on the as-produced and calcined apatite powders by the KBr method (A-IIItype, Jasco Co. Tokyo, Japan). The specific surface area of the as-produced powder was measured by the Braunauer-Emmett-Teller (BET) method (Flowsorb 2300, Shimadzu Co. Kyoto, Japan). The shape and size of the apatite powder were observed by transmission electron microscopy (Hitachi H-700H, Hitachi Co. Tokyo, Japan) at an acceleration voltage of 200 kV. The true density of the apatite powder dried at 100°C was measured by the pycnometer method using kerosine.

Results and Discussion

Formation of hydroxyapatite

Figure 1 shows the change in pH of the 0.5 M calcium hydroxide suspension during the addition of the 0.3 M orthophosphoric acid solution (added amount: 100 ml). Samples A and B provided a similar pH change for the addition rate of 1 ml/minute of H_3PO_4 solution. The pH of the $Ca(OH)_2$ suspension was kept almost constant in value by the addition of 60 ml of H_3PO_4 solution. A further addition of H_3PO_4 solution decreased drastically the pH of $Ca(OH)_2$ suspension. Finally, the suspension pH reached 6.8 after the

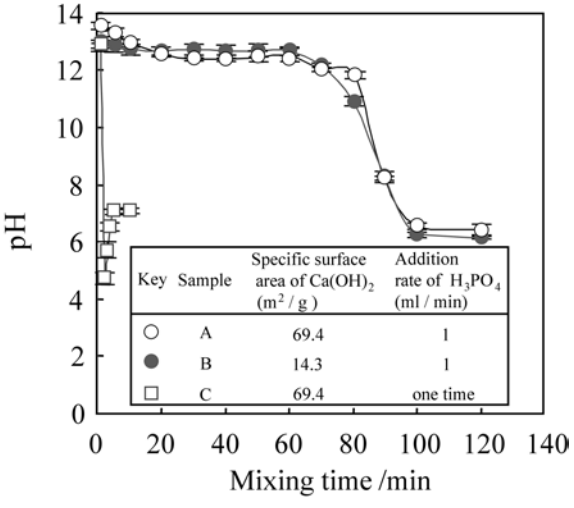

Fig. 1. Change in pH of 0.5 M $Ca(OH)_2$ suspension during the addition of 0.3 M H_3PO_4 solution (100 ml) at room temperature.

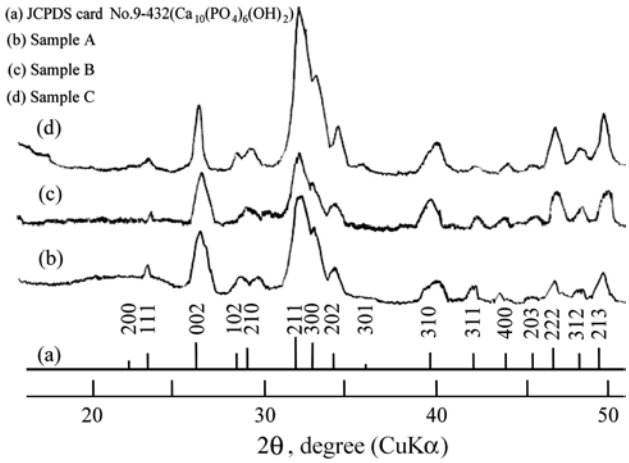

Fig. 2. X-ray diffraction patterns of hydroxyapatite formed from 0.5 M $Ca(OH)_2$ suspension and 0.3 M H_3PO_4 solution and presented in JCPDS card No. 9-432. See Fig. 1 for samples A, B and C.

complete addition of the H_3PO_4 solution. This result suggests that continuous dissolution of $Ca(OH)_2$ powder supplies OH^- ions to keep the pH value high during the formation of hydroxyapatite particles from the supersaturated Ca^{2+} ions and added PO_4^{3-} ions. Further formation of apatite particles consumes the Ca^{2+} and OH^- ions remaining in the suspension and decreases gradually the concentration of OH^- ions in the reaction range from 50 to 100% of $Ca(OH)_2$ powder. When 100 ml of 0.3 M H_3PO_4 solution was added in one batch (sample C), the pH of the suspension dropped to 4.9 and rose again to 7.2 over a short time. This result indicates that a rapid reaction proceeded among dissolved Ca^{2+} ions, OH^- ions and added H_3PO_4 solution to form apatite particles. The recovery of pH to 7.2 corresponds to the dissolution and reaction of the remaining $Ca(OH)_2$ particles.

Figure 2 shows the X-ray diffraction patterns of solids formed in samples A, B and C, and hydroxyapatite in JCPDS card (No. 9-432). The diffraction patterns of the synthesized samples were in accordance with those of hydroxyapatite, indicating no effect of specific surface area of the $Ca(OH)_2$ particles and mixing rate of the H_3PO_4 solution on the formation of crystalline hydroxyapatite. Table 3 shows the size of apatite crystallites, measured on the diffraction line (002). The crystallite size depended on the concentrations of the starting $Ca(OH)_2$ suspension and the H_3PO_4 solution. An increase in the concentrations of the starting raw materials decreased the crystallite size of the hydroxyapatite because of the increased nucleation rate of hydroxyapatite. As seen in the data for samples A and B, the size (specific surface area) of the starting $Ca(OH)_2$ had no influence on the crystallite size.

Table 3. Influence of the concentration of starting materials on the crystallite size of synthesized apatite particles

	Concetraton of $Ca(OH)_2$ (M)	Concetraton of H_3PO_4 (M)	Crystallite size (nm)
sample A	0.5	0.3	40.8
	1.0	0.6	36.5
	2.0	1.2	16.9
	3.0	1.8	16.2
sample B	0.5	0.3	42.1

Figure 3 shows IR spectra of the hydroxyapatite produced in samples A and B, dried at 100°C and heat-treated at 600°C. In Fig. 3, the IR spectrum of commercial hydroxyapatite powder of specific surface area 13.2 m^2/ g (Taihei Chemical Industrial Co. Ltd. Osaka, Japan) is also presented. All the spectra represent the stretching vibration of the OH group at 3550 cm^{-1} and the stretching vibration of the PO_4 group at 603 and 1051 cm^{-1}. No significant difference in the IR spectra with heating was measured.

Specific surface area and particle size

Figure 4 shows (a) the specific surface area and (b) diameter of the equivalent spherical particle for hydroxyapatite samples A, B and C and the commercial powder. The measured specific surface area was converted to the particle diameter using a true density of 3.14 g/cm^3, which was measured for sample A. The multiple data represent the reproducibility of the synthesis of the apatite powder from an 0.5 M $Ca(OH)_2$ suspension and an 0.3 M H_3PO_4 solution. Samples A, B and C gave specific surface areas in the range 45-58, 42-63 and 39-69 m^2/g, respectively. The reproducibility of synthesis experiments was relatively lower for sample C where the raw materials were mixed once. However, it was found that the apatite powders synthesized in this experiment have significantly higher values of specific surface area as compared with the commercial powder. The equivalent diameters of hydroxyapatite particles

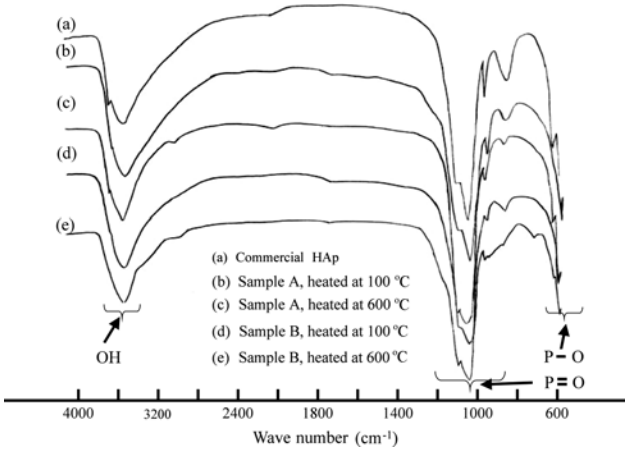

Fig. 3. Infrared spectra of hydroxyapatite after drying at 100°C and heat-treatment at 600°C. See Fig. 1 for samples. The infrared spectrum (a) represents the commercial hydroxyapatite powder with specific surface area 13.2 m^2/g.

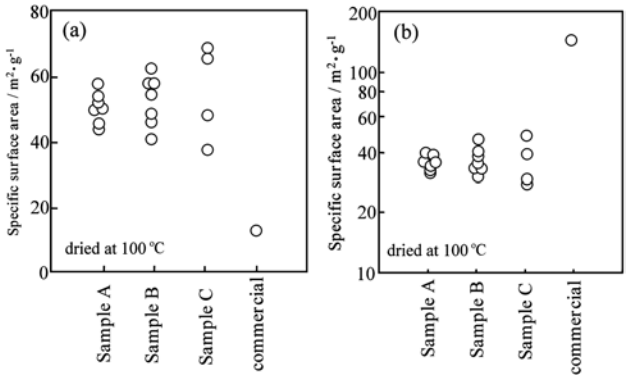

Fig. 4. Specific surface area (a) and corresponding equivalent particle diameter (b) of hydroxyapatite formed from 0.5 M $Ca(OH)_2$ suspension and 0.3 M H_3PO_4 solution and commercial hydroxyapatite powder.

produced in samples A, B and C were in the range of 33-42, 30-46 and 28-49 nm, respectively. The similar particle sizes between samples A and B in Fig. 4(b) supports the formation mechanism of hydroxyapatite particles through reaction between the dissolved Ca^{2+} and OH^- ions. Figure 5 shows the effect of the concentration of the $Ca(OH)_2$ suspension on (a) the specific surface area and (b) the corresponding equivalent diameter of the apatite powder produced. An increase of the $Ca(OH)_2$ concentration leads to the formation of ultrafine apatite particles with a high specific surface area. This tendency agreed with the change in crystallite size of hydroxyapatite with the concentration of the $Ca(OH)_2$ suspension (Table 3). An increased nucleation rate of hydroxyapatite causes the decrease of particle size.

Figure 6 shows transmission electron micrographs of hydroxyapatite particles in (a) sample A and (b) sample B produced from an 0.5 M $Ca(OH)_2$ suspension and an 0.3 M H_3PO_4 solution. It is difficult to identify primary particles but both round and needle-shape particles were observed. The diameter of round particles was 25-70 nm. The length and width of needle-shape particles

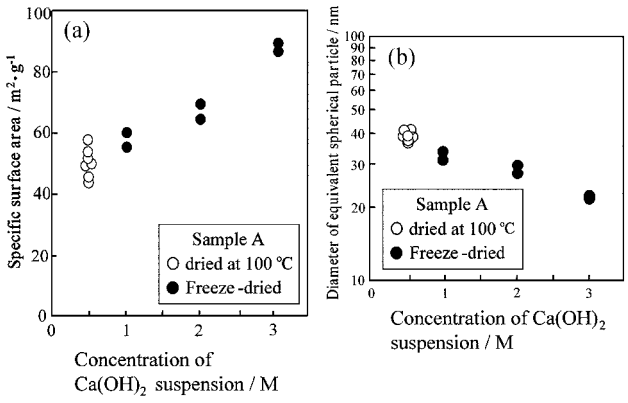

Fig. 5. Effect of the concentration of $Ca(OH)_2$ suspension on (a) specific surface area and (b) corresponding equivalent diameter of produced apatite powders.

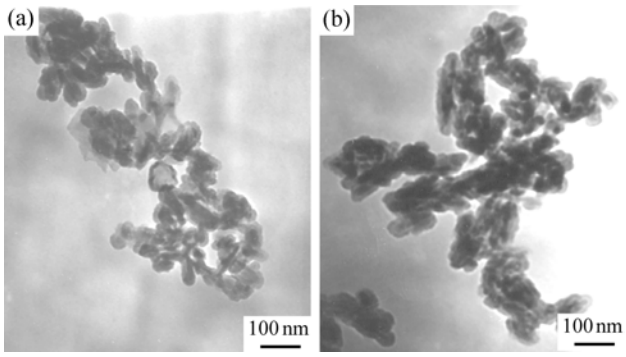

Fig. 6. Transmission electron micrographs of hydroxyapatite particles in (a) sample A and (b) sample B produced from 0.5 M $Ca(OH)_2$ suspension and 0.3 M H_3PO_4 solution.

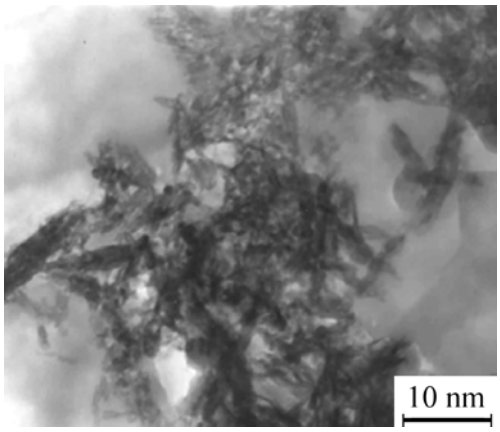

Fig. 7. Ultrafine needle-shape hydroxyapatite particles produced in sample A from 2.0 M $Ca(OH)_2$ suspension and 1.2 M H_3PO_4 solution.

were in the range of 50-100 nm and 20-40 nm, respectively. These particle sizes were comparable to the diameters from specific surface areas (Fig. 4(b)). Figure 7 shows clearly the formation of ultrafine needle-shape hydroxyapatite particles of 10 nm length, produced in sample A from a 2.0 M $Ca(OH)_2$ suspension and a 1.2 M H_3PO_4 solution. An increase of the concentrations of raw materials leads to the formation of needle-shape apatite particles rather than round-shape particles.

Conclusions

(1) The ultrafine hydroxyapatite particles with a 20-50 nm equivalent spherical particle diameter were produced by the reaction among Ca^{2+} and OH^- ions dissolved from $Ca(OH)_2$, and added H_3PO_4 solutions at room temperature.

(2) An increase in the concentrations of starting raw materials decreased the crystallite size and the primary particle size of hydroxyapatite produced, and promoted the formation of needle-shape apatite particles.

(3) The specific surface area of the starting $Ca(OH)_2$ powder had no influence on the crystallite size and specific surface area of apatite particles produced.

References

[1] T.S.B. Narasaraju and D.E. Phebe, J. Mater. Sci. 31 (1996) 1-9.
[2] T. Kokubo, Bull. Ceram. Soc. Japan 30 (1995) 223-229.
[3] M. Akao, Bull. Ceram. Soc. Japan 20 (1985) 1096-1103.
[4] T. Kawai and Y. Waseda, Metal Material 65 (1995) 675-684.
[5] E. Bouyer, F. Gitzhofer and M.I. Boulos, J. Mater. Sci. 11(2000) 523-531.
[6] Y. Suwa, H. Banno, M. Mizuno and H. Saito, J. Ceram. Soc. Japan 101 (1993) 659-664.
[7] M. Wei. A.J. Ruys, B. Kmilthorpe and C.C. Sorrell, J. Biomed. Mater. Res. 45 (1999) 11-19.
[8] L. Qi, J. Ma, H. Cheng and Z. Zhao, J. Mater. Sci. Lett. 16 (1997) 1779-1781.
[9] D.M. Liu, Q. Yang, T. Troczynski and W.J. Tseng, Biomaterials 23 (2002) 1679-1687.
[10] D.B. Assollant, A. Ababou, E. Champion and M. Heughebaert, J. Eur. Ceram. Soc. 23 (2003) 229-241.